Journal of Power Sources 272 (2014) 45–57

Contents lists available at ScienceDirect

Journal of Power Sources

journal homepage: www.elsevier.com/locate/jpowsour

Calendar ageing analysis of a $LiFePO_4$/graphite cell with dynamic model validations: Towards realistic lifetime predictions

E. Sarasketa-Zabala*, I. Gandiaga, L.M. Rodriguez-Martinez, I. Villarreal

IK4-Ikerlan, Energy Business Unit, Arabako Teknologi Parkea, Juan de La Cierva 1, E-01510 Miñao, Spain

HIGHLIGHTS

- Detailed analysis of the influence of temperature and state of charge (SOC) on cell ageing upon storage.
- Calendar-lifetime prediction based on identified main ageing phenomena.
- Static and dynamic model validations (under constant and non-constant parameters profiles, respectively).
- Simulations of real application scenarios.

ARTICLE INFO

Article history:
Received 20 May 2014
Received in revised form
18 July 2014
Accepted 13 August 2014
Available online 23 August 2014

Keywords:
Li-ion battery ageing
$LiFePO_4$ (LFP)/graphite
Calendar-life performance model
Dynamic storage profiles
Lithium inventory loss (LLI)

ABSTRACT

The present study aims at establishing a methodology for a comprehensive calendar ageing predictive model development, focusing specially on validation procedures. A LFP-based Li-ion cell performance degradation was analysed under different temperature and SOC storage conditions. Five static calendar ageing conditions were used for understanding the ageing trends and modelling the dominant ageing phenomena (SEI growth and the resulting loss of active lithium). The validation process included an additional test under other constant operating conditions (static validation) and other four tests under non–constant impact factors operating schemes within the same experiment (dynamic validation), in response to battery stress conditions in real applications. Model predictions are in good agreement with experimental results as the residuals are always below 1% for experiments run for 300–650 days. The model is able to predict dynamic behaviour close to real operating conditions and the level of accuracy corresponds to a root-mean-square error of 0.93%.

1. Introduction

The existing wide range of battery technologies nowadays can be grouped into lead, nickel, lithium, sodium and flow battery families. Others, such as high temperature batteries, as well as new developments based on lithium air, are in a distant state of development to meet market specifications in various sectors. Lithium-ion (Li-ion) technology is which most has progressed in recent years, capturing over half of the sales value of secondary consumer market (portable equipments). Moreover, it is a promising candidate for large scale applications due to its large energy and power densities. The commitment of battery manufacturers and automotive companies to develop Electricity Storage Systems (ESS) based on Li-ion technology for new generations of Hybrid and Electric Vehicles (HEV and EV) is making possible the reduction in manufacturing costs and therefore the continuous development of this technology. However, the long cell lifetime and performance required for automotive applications (*ca.* 10 years) is still uncertain for Li-ion batteries.

Both cycling and storage performance are key issues for Li-ion battery (LIB) applications. Hence, analysing the ageing during both cycling and storage is necessary for understanding capacity and power fade over time. The storage ageing represents an important factor, taking into account that, for instance, a personal car spends about 90–95% of its lifetime in storage mode when parked [1,2] or that most Uninterruptible Power Supplies (UPS) are only used a few minutes over their lifetime, just when the mains power fail. Hence, the relevance of investigating cell degradation in the course of the time in storage mode is high for many applications, and this is the definition for calendar life in the present paper.

There are several calendar ageing studies in the literature [1–52] for different LIB technologies based mainly on: NMC

* Corresponding author. Tel.: +34 945 297 032; fax: +34 945 296 926.
E-mail address: esarasketa@ikerlan.es (E. Sarasketa-Zabala).

http://dx.doi.org/10.1016/j.jpowsour.2014.08.051
0378-7753/

($LiNiMnCoO_2$), NMC-LMO ($LiNiMnO_2$–$LiMn_2O_4$), NMO ($Li(NiMn)_2O_4$), LFP ($LiFePO_4$), LCO ($LiCoO_2$), LNCO ($LiNiCoO_2$) and NCA ($LiNiCoAlO_2$). Standing period (t), State of Charge (SOC) and temperature (T) are factors that affect the calendar lifetime and charge retention of the battery. Degradation processes not only depend on storage conditions but also strongly on electrolyte and electrodes active materials [53–55]. Table 1 shows a literature review of main calendar ageing analyses on several LIB technologies (physical approaches are out of scope and survey is focused on commercial and prototype batteries). Some authors [4,7,8,17,21,25] studied both calendar and cycling individually and compared the corresponding ageing results under similar SOC and T conditions. M. Ecker *et al.* [18] validated the calendar ageing model under static cycling operation, aiming at verifying whether the developed model would be able to predict cycling ageing. They also combined the calendar semi-empirical approach with impedance-based electro-thermal model for a complete lifetime model. J. Schmalstieg *et al.* [42] used the calendar ageing study to develop a holistic ageing model. Their overall model validation was based on different realistic driving profiles and temperatures. D. Stroe *et al.* [56] showed calendar lifetime extrapolations as part of a methodology for lifetime prediction. They did not either include calendar model validation steps and they proposed an application specific mission profile to verify the overall lifetime model. All in all, none of the studies focused on single semi-empirical calendar ageing models validation and did not check the model capability to predict the cell operation under non-constant storage SOC and temperature operation conditions.

LFP cathode based LIBs are of high interest for high power applications (*e.g.* HEV) because of LFP active materials [57–65]:

- Safe performance due to a high thermal stability
- Low cost and toxicity compared to cathodes such as LCO
- High specific power (LFP cathode has a theoretical capacity of 170 mAh g^{-1} and redox potential around 3.43 *vs.* Li electrode [5])
- High cycling capability due to stable olivine-type chemical structure

It is one of the most capable Li-ion cell type considering safety and production cost [66]. However, the lifetime is still uncertain. LFP-based large size LIBs calendar ageing studies are various in the literature [2,5,9,22,38,44]. Only S. Grolleau *et al.* [2] validated the calendar model under dynamic storage conditions, but they just focused on temperature impact factor. Several studies took also into account cycle ageing [9,22,38,44], but they did not pay special attention to the combined complex effects of both operation modes. In this sense, after reviewing the state of the art, the present calendar ageing analysis enhances the results by adding further steps of dynamic validation and combining the results of calendar ageing with those from cycling ageing following a fully semi-empirical approach.

Table 1
Overall calendar lifetime prediction worldwide activity.

Type of analysis		Reference
Non-destructive electrical and/or electrochemical characterisation, sometimes including fitting		[1–5,7,8,10,11,13,14,17–45]
Post-mortem analysis		[6,9,10,12,16,19,28,31,38,41,44–51]
- Understanding of impact factors effect		[5,17,21,22,32,36,43,48,52]
- Studying ageing phenomena		
Dynamic behaviour analysis	Cell voltage	[17]
	Temperature (validation test)	[2]

A methodology for lifetime prognosis has been developed, which comprises both cycle and calendar ageing but also their interaction in depth analysis. The main overall objective of this work includes the development of validation procedures for both ageing types models and the analysis of applicability of the methodology [67]. As part of a comprehensive lifetime analysis procedure, this paper aims specifically at studying cell performance degradation under different temperature and SOC storage conditions and developing a thoroughly validated semi-empirical calendar ageing predictive model. The selected reference for this investigation work is a commercial LFP/graphite 26650-type cell with 2.3 Ah nominal capacity. The process defined for calendar lifetime analysis is shown in Fig. 1. In this paper, the steps within the shadowed area are covered. The validation process not only consisted in additional tests under other constant operating conditions (static validation) but also under non-constant impact factors operating schemes (dynamic validation), as battery stress conditions in real applications are barely constant over time. It is therefore essential developing predictive tools that enable evaluating the degradation under different stress levels operating conditions [68]. Thus, predictions were performed comparing with experimental data upon storage under variable environment T and/or SOC conditions on the same cells over time. Finally, the calendar-life performance of the studied reference was also evaluated in a UPS application.

2. Experimental

The performance of a commercially available LFP/graphite 26650-type cell, designed for high power applications, was evaluated. Single-factorial variation experiments were carried out using cells of the same manufacturing batch with 2.3 Ah nominal capacity and 3.3 V nominal voltage. For each storage test a single cell was used, as in a previous study using the same reference it was measured that the average coefficient of variation upon ageing was just 6% using 3 cells per condition.

The ageing tests were performed in a temperature-controlled environment. CTS and Prebatem climatic chambers were used with this purpose. The periodical check-up experiments were carried out using Digatron multiple cell tester with data adquisition BTS-600 software. Electrochemical Impedance Spectroscopy (EIS) measurements were conducted using Digatron EISmeter Impedance Spectroscope.

2.1. Experimental procedures

Fig. 2 shows the flow chart for the testing procedure including both State of Health (SOH) controlling steps and accelerated storage ageing tests. The latter (boxes in blue) are described in section 2.2. Both capacity (Q) loss and internal resistance (IR) increase were measured in order to evaluate cell SOH over time and parameterise battery ageing model. Intermittent Electrical Parameters Identification Tests (EPIT) were carefully planned so that their impact on cell degradation was as negligible as possible. These tests were carried out at room temperature (25 °C) as follows:

- *Actual nominal capacity* (*Q*) *measurement*: charge–discharge cycles (constant current-constant voltage, CC–CV, and CC modes, respectively) at nominal conditions specified by cell manufacturer (1C in CC mode). Three full charge–discharge cycles were performed in order to assess both reversible and irreversible capacity losses and check the repeatability of the results.
- *Close to equilibrium Open Circuit Voltage* (*quasi-OCV*) *measurements*: cell full discharge at C/5 low C-rate. This C-rate was

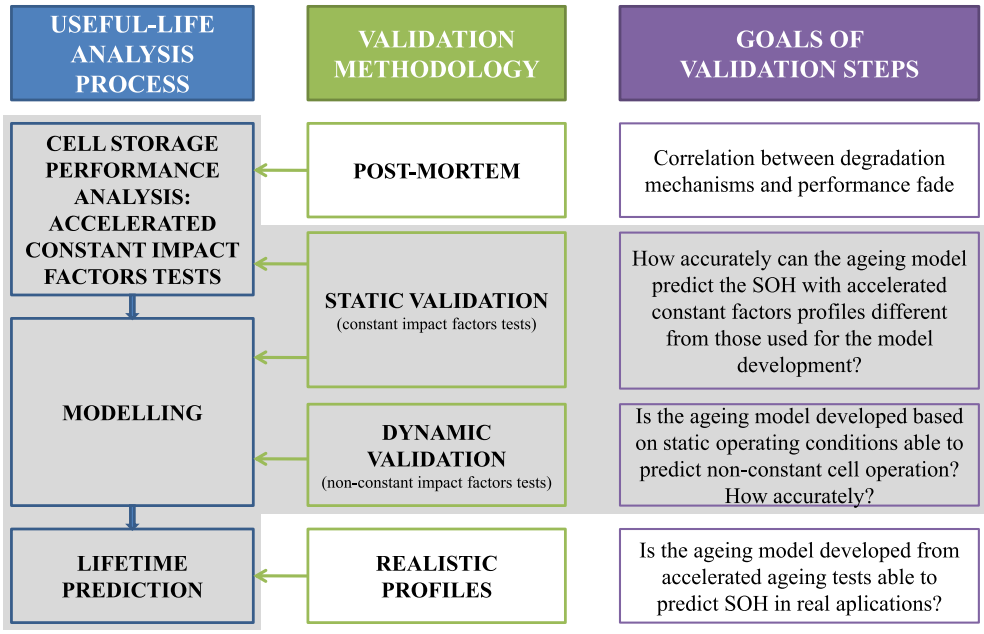

Fig. 1. Methodology for calendar lifetime prognosis.

chosen as it was the largest one that enabled observing the voltage plateaus of the cell. Galvanostatic voltage profiles traced accurately with cell SOC were used for examining electrode phase changes and understanding degradation phenomena.

- *Actual Direct Current* (*DC*) *IR measurement* (*Hybrid Pulse Power Test*, *HPPT*): current pulses at cell maximum acceptable charge and discharge C-rates over cell 90–20% SOC range with 10% ΔSOC intervals.

The first step, *i.e.* cell conditioning, consisted of formation–reactivation cycles carried out following the same procedure as for the nominal capacity test. Additionally, both Beginning of Life (BOL) and cell further characterisation tests at End of Test (EOT) included:

- *EIS measurements*: impedance change evaluation in galvanostatic mode using frequency range from 0.1 Hz to 6.5 kHz at 25 °C at 30% and 70% cell SOC. This test was also included occasionally in EPIT.
- *Rate capability tests*: operating discharge and charge capacity measurements at 5, 25 and 45 °C were performed at two charge and discharge C-rates. The charging C-rate was 3C and the discharging one 6.5C. Operating charge capacities were evaluated at CC mode at the different specified conditions previously discharging the cell up to cut-off voltage at 1C and 25 °C. Operating discharge capacities were determined at the different specified conditions after fully charging the cell (in CC–CV mode) at 1C and 25 °C. Each testing condition was repeated 3 times in order to check the repeatability of tests and evaluate average results.

2.2. Accelerated ageing tests conditions

2.2.1. Calendar ageing and static validation tests

Calendar ageing was initially investigated at several but constant T and SOC storage conditions over time on the same cell, as shown in Table 2. Five different storage conditions were used for calendar ageing model development and an additional one at 50 °C and 90% SOC for the static validation (shaded in Table 2). Range limits for the tested external influence factors were chosen within the cell operation window set by the manufacturer. Nonetheless, outer limits were not checked since a real-life application may not operate in such conditions. Ageing tests were carried out correcting the values of set SOC parameter according to cell actual capacity after every EPIT. Cells were stored at open circuit (OC) in order that reversible capacity loss rates could be evaluated as a function of impact factor levels, storing period and accumulated irreversible capacity fade. Even though OC storage mode could in principle imply a drawback for ageing predictive models development, other authors reported that self-discharge is of minor importance below 100% SOC [17]. Even though this latter ageing study was of an NMC-based LIB, self-discharge of Li-ion cells is mostly due to delithiation of graphite and Solid Electrolyte Interface (SEI) formation at graphite surface [69].

2.2.2. Dynamic validation tests

Additional tests under variable environment temperature and/or SOC conditions within each cell were carried out aiming at the validation of the calendar ageing model under different stress levels operating conditions. The tested four operating schemes with non-constant impact factors are shown in Fig. 3. Temperature was made dynamic upon storage for three of them and SOC in one of the tests (in red, in the web version).

3. Results and discussions

The results from ageing tests are used to understand cells behaviour upon different storage conditions and to develop a comprehensive calendar lifetime predictive model. Main evaluated parameters are discussed in the following section.

3.1. Cell performance fade evaluation

- Analysis of ageing results

The measured nominal capacity at the BOL was 2.331 ± 0.014 Ah (95% confidence interval, CI). Charging/discharging voltage responses at different ageing stages were analysed aiming at

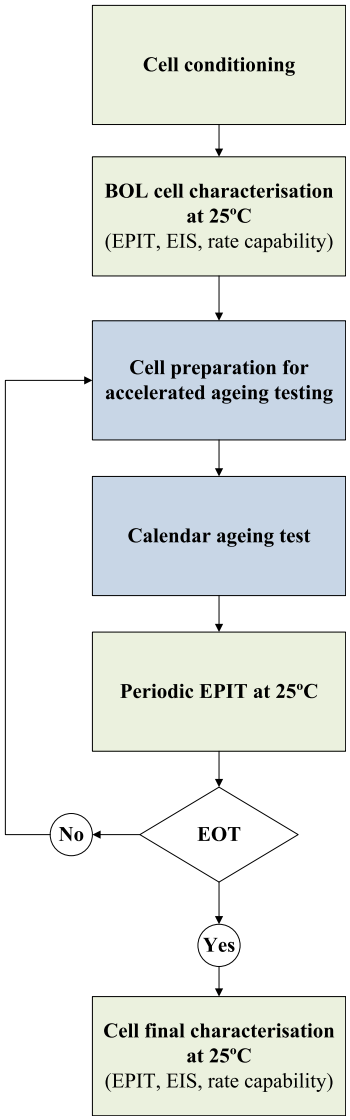

Fig. 2. Testing procedure used for ageing tests.

identifying the contributions of irreversible capacity loss and IR increase. Fig. 4 shows the charge–discharge curves at 1C and 25 °C after similar storage periods under different conditions (Table 2). Similarly to reported in Refs. [5], it was observed that calendar-life is more affected by elevated temperature than by SOC. In general, there is a shift in discharge curves to lower actual capacity values as time increases. The length of the plateau part is shortened, which indicates capacity loss due to loss of active lithium (LLI) [70]. The voltage plateau, which corresponds to the nominal voltage of the cell, was in general just slightly shifted to lower voltages as the cells aged, indicating that the contribution of IR increase on cell performance change was of no significance [70,71]. However, at 50 °C and 70% SOC, the contribution of IR factor is more marked after

Table 2
Test matrix for calendar ageing modelling (static validation highlighted in grey).

T [°C]	SOC [%]		
	30	70	90
30		X	
40	X	X	X
50		X	X

*ca.*19 months of storage. Hence, the ohmic resistance and charge transfer resistance may have become larger over time at such high temperature. The duration of CC charge mode time also decreased with storage, while the IR increase was negligible, so the SOH of the studied LFP/graphite cell is mainly connected with the available active lithium inventory. Hence, the main cause of ageing may be the decomposition of the electrolyte and the resulting growth of SEI layer due to deposition of decomposition products on graphite anode surface. In the case of the 50 °C and 70% SOC storage condition, electrolyte degradation and the progressive increase of the thickness of the passivating layer probably contributed to IR increase.

Fig. 5 shows DC IR increase over time during different cell storing conditions together with the corresponding capacity losses, which are represented according to the most extended criteria for the End of Life (EOL) in the literature, *i.e.* 80% SOH (Q) and 200% SOH (IR). That is to say, the measured capacity loss was adjusted to the common scale of the EOL by translating 20% capacity loss to 100% scale so that both ageing metrics could be compared within the useful lifetime of the cell. Area in red (in the web version) in Fig. 5 represents cell state over this EOL definition. DC IR change during discharge at 50% SOC is just shown because, as reported in a previous work [67], regardless of DC IR testing procedure (HPPT), *i.e.* charge or discharge current step and reference voltage, the measured IR change trend was similar. As plotted in Fig. 5, an unexpected slight initial decrease of IR was observed, in agreement with other studies with similar cells [22,72]. The moderate increase of total resistance suggests that bulk transport properties are almost unchanged over storage (absence of structural degradation) [5]. According to [70,73], if the battery impedance does not increase rapidly compared to capacity loss, the battery behaviour is stable with temperature. The capacity loss rate became steady over time, which is in agreement with the expected lithium ions consumption during SEI layer growth. However, during 50 °C storage (70% SOC), after approximately a year both capacity loss and IR increase evolution were altered clearly. Such cell ageing trend change is known to be related to the less active electrode area that limits cell performance [74]. All in all, both Figs. 4 and 5 show that the investigated LFP-based cell was aged primarily due to capacity fade rather than power fade, as also reported by other authors [22,71,72].

The influence of IR on cell performance was also evaluated by means of charge–discharge-rate capability tests at different temperatures at BOL and after different ageing conditions at the EOT. Fig. 6 aims at evaluating cells rate capability at different SOH due to the storage at different temperatures during the same period of time. Hence, the results corresponding to cells that were stored at 30 °C, 40 °C and 50 °C for *ca.* 21 months are discussed, with a SOH of, referred to capacity, 93%, 88.5% and 77.9%, respectively (actual nominal capacity normalised to the nominal capacity at BOL). Fig. 6 represents, for the selected aged specimens and BOL condition, as reference: (i) the charged capacity at 3C in CC mode (Fig. 6(a)) and discharge capacity at 6.5C (Fig. 6(b)), both normalised to cell actual nominal capacity (at 1C) (coloured areas), (ii) the charging time in CC mode under different conditions (Fig. 6(a)), and (iii) the cell surface temperature total change during charge and discharge measured with Type K thermocouples in each case (line of columns and right axis of abscissas) in both figures. Operating capacity data at 45 °C is not shown in Fig. 6(b) because the outcomes were not comparable, as all the tested specimens could not be fully discharged (up to the cut-off voltage) due to large surface temperature increase above the maximum temperature safety limit. Operating capacity data, in percentage, already show changes in cell current dependency upon polarisation effects.

The ambient temperature had a significant influence on cell regenerative operation (Fig. 6(a)). At 25 °C, there was virtually no

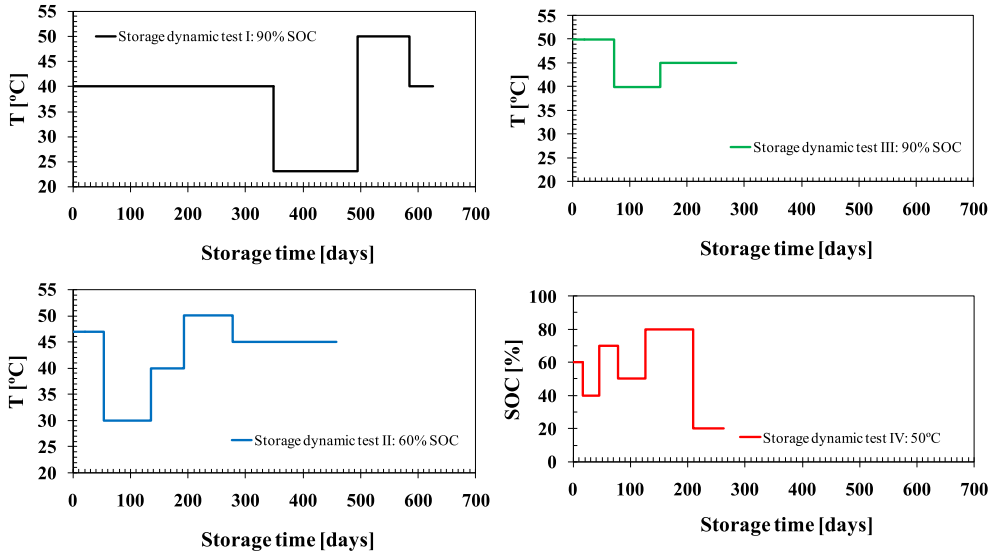

Fig. 3. Dynamic storage tests. Dynamic T and SOC profiles over time.

change in the charging capability among the BOL cell and the aged cells stored at 30 and 40 °C. The retention of charge rate capability suggests a negligible increase of cell resistance upon storage, as demonstrated above, but also non-remarkable deterioration of LFP electrode [5], since LFP-based LIB on charge is limited by lithium removal from the LFP cathode. The difference between initial state and after ageing at 50 °C was very small, the Ampere-hours that the cell could accept just reduced 2.8%. The influence of this cell IR increase on charge capability was not apparently large, as the increase of cell charging percentage was not particularly enhanced from 25 to 45 °C ambient temperature testing, in all cases *ca.* 8%, even though elevated temperature favours rate of lithium intercalations–deintercalation kinetics. At 5 °C with slow lithium ion diffusion, the operating voltage was reduced and, therefore, the more aged the cell, the less charge the cell could accept. The temperature change on the most aged cell was so small because it was hardly charged. According to S.S. Zhang *et al.* [75], poor low temperature performance is related to low diffusivity of lithium, but high charge-transfer resistance of delithiated graphite and lithiated cathode upon cell charging may also affect it. The ionic conductivity of electrolyte and SEI layer on graphite surface may be especially reduced in the case of the cell that had been stored at 50 °C. Hence,

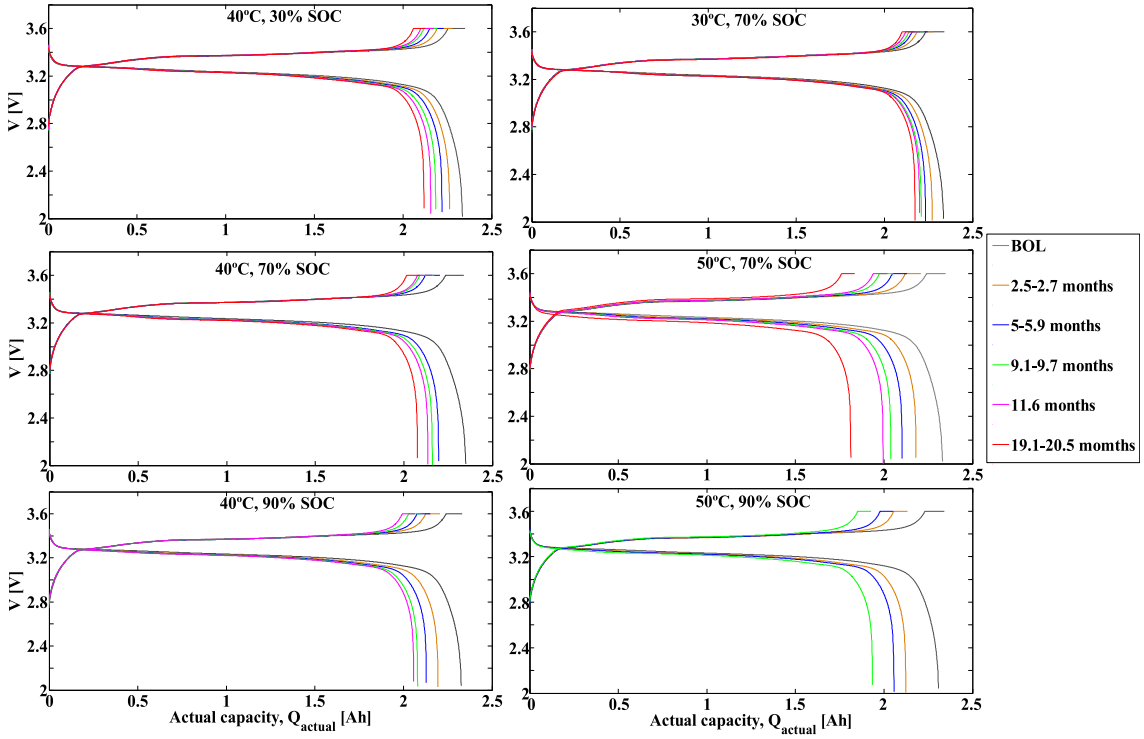

Fig. 4. Charge-discharge curves at 1C and 25 °C for the different ageing stages of the cells stored at different SOC and T conditions. Charge-discharge profiles from nominal capacity measurements.

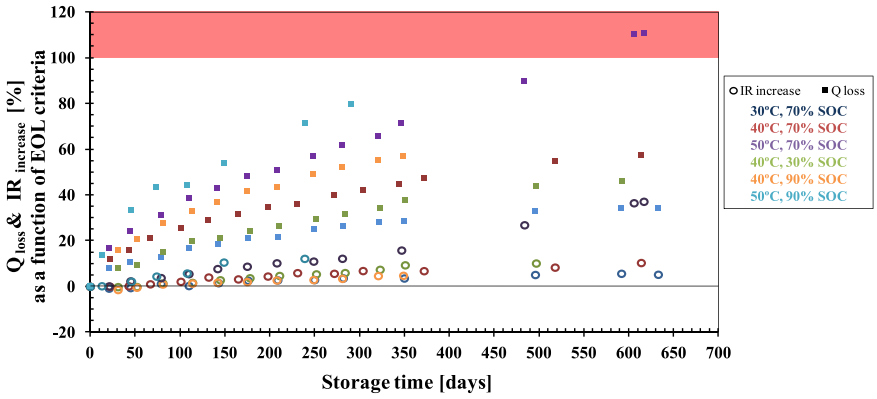

Fig. 5. DC internal resistance increase ($IR_{increase}$) and capacity loss (Q_{loss}) adjusted to EOL scale over time (both Q and IR were normalised to initial nominal values).

its poor regenerative performance at low temperature may be the consequence of high electric polarisation.

At 6.5C current load and 25 °C discharge conditions (Fig. 6(b)), it was possible to withdraw almost the total Ampere-hours charged in cells that had been stored at 30 and 40 °C (99–99.5%). The cell aged at 50 °C provided just 1.5% less capacity than the BOL cell reference. The thermal behaviour was similar in all cases because of the lower discharge times to reach the cut-off voltage (the stored capacity was 7%, 11.5% and 22.1% lower for the cells stored at 30, 40 and 50 °C, respectively, than in BOL cell). The rate capability on discharge might have been maintained due to significant LLI. Lower Li intercalation into the graphite anode restricts the operation window of LFP electrode. At lower maximum lithium stoichiometry, the rate capability of the cell is larger [22,74]. The results demonstrated that at room temperature the discharged capacity barely depends on the C-rate (discharge at 1C and 6.5C was almost equal). At 5 °C, cells that had been stored at 30 and 40 °C underwent a slight decrease of 0.9–1% in discharged capacity when compared to the BOL cell, whereas the difference increased up to 5.9% for the cell that was stored at 50 °C. This is related not only to LLI but also to this latter cell higher overall resistance. Its charge transfer resistance may have increased and electronic and ionic conductivity modified. The suffered polarisation was remarkably higher in the discharged state of the cell (Fig. 6(a)). Charging of a discharged Li-ion battery is more difficult than discharging a charged battery at low temperature [75].

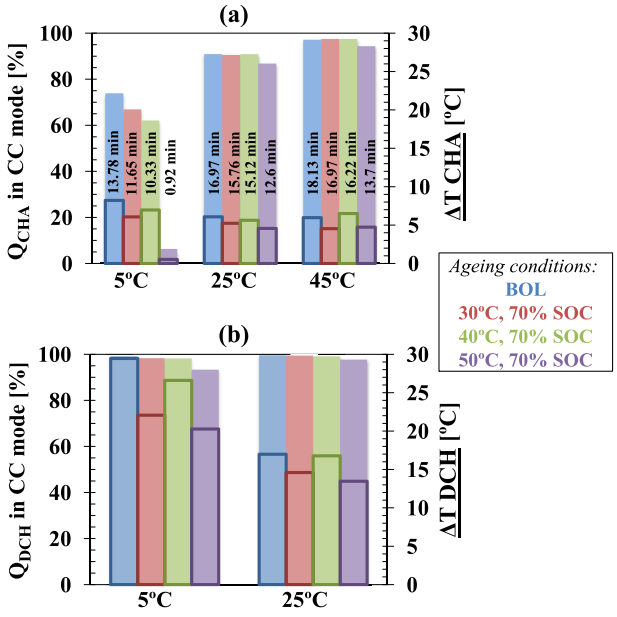

Fig. 6. Charge and discharge rate capability (Q_{CHA} and Q_{DCH}, coloured areas) and cell surface temperature change (ΔT, line of columns) on charge at 3C (a) and discharge at 6C (b) at different temperatures at BOL and after storage under different temperature conditions during *ca.* 20 months. CC charging time is indicated for each condition in (a).

Overall, Figs. 4,5 and 6 demonstrate that there was negligible increase of cell resistance upon storage, LLI was dominant ageing phenomenon and LFP electrode might not be degraded. In the case of 50 °C and 70% SOC storage condition, after prolonged storage time the LLI was not any more stable, and it was accompanied by cell impedance change, indicating ageing processes modification.

- Self-discharge

Total capacity loss of cells stored at OC was evaluated, meaning both irreversible capacity loss and cell reversible capacity loss, as side reactions also lead to self-discharge of the cell. Reversible capacity loss (self-discharge) was analysed for each storage period between EPITs, whereas irreversible capacity loss was considered accumulative over time. Fig. 7 presents the corresponding results for the different storage conditions (comparative reversible and irreversible capacity loss data). The self-discharge rate is expected to evolve with ageing [7]. However, the reversible capacity loss was approximately constant regardless the irreversible capacity loss increase over time, although it changed depending on storing time step duration (Δt). It was initially larger than after overall prolonged storing time. The effect of storing temperature and SOC on reversible capacity loss, as shown in Fig. 8, was also assessed. Self-discharge rate increased with storing SOC (Fig. 8(a)). Higher SOC resulted in lowering the anode potential, which causes electrochemical instability on electrolyte material. Intercalated lithium in lithiated graphite tends to diffuse to the edges where it may interact with solvent components [76]. There was no clear temperature dependency on cell reversible capacity loss (Fig. 8(b)), even though it is recommended storing batteries below room temperature (ideally 15 °C) because of low self-discharge rates and slow ageing processes. On the contrary, both stress factors (SOC and T) effects were appreciable on irreversible capacity loss. The higher both SOC and T, the larger the capacity fade upon storage (Fig. 7). After *ca.* 10 months of storage, at 40 °C, the irreversible capacity loss was 6.4%, 8% and 10.5% at 30%, 70% and 90% SOC, respectively. At 70% SOC, capacity decreased by 5.3%, 8% and 12.4% at 30 °C, 40 °C and 50 °C, respectively.

The demonstrated low self-discharge rate was related to the stable SEI layer growth (Fig. 5, before the ageing rate increased at

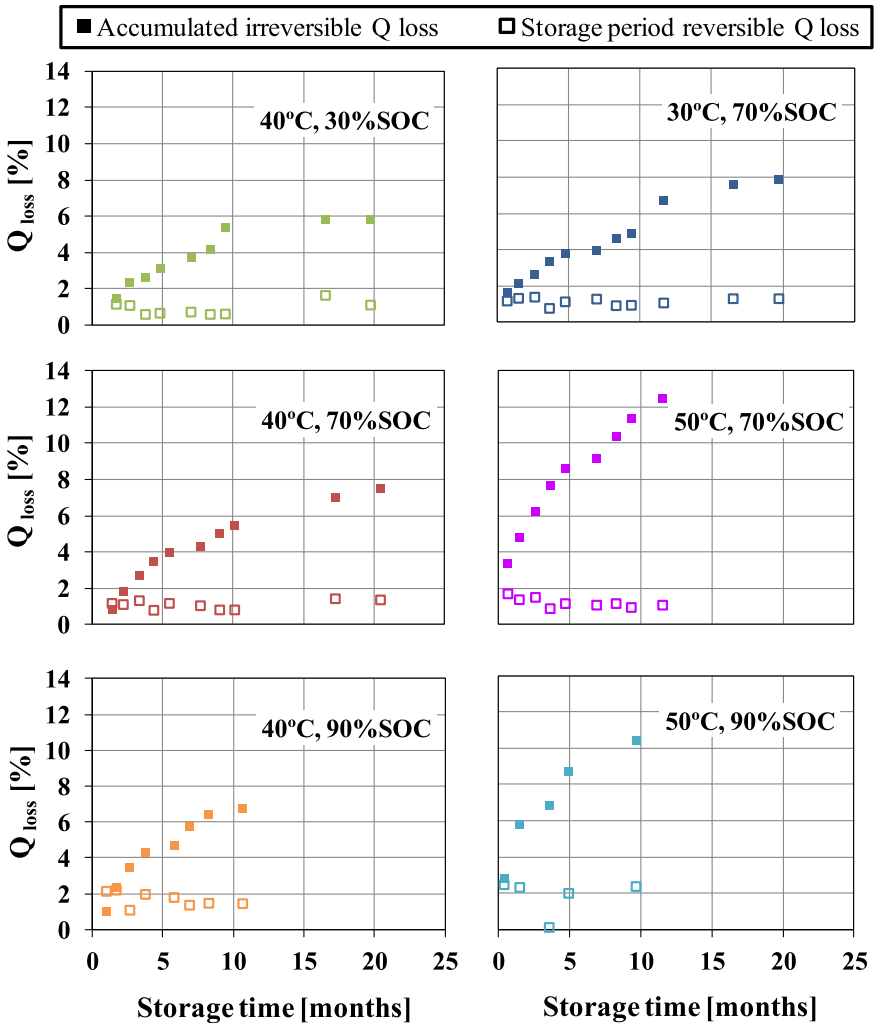

Fig. 7. Reversible time step capacity loss and accumulated capacity loss (Q_{loss}, both normalised to initial nominal values) of the cells stored at different OC conditions assessed from the nominal capacity test.

50 °C and 70% SOC), as electrolyte solvents that enable the formation of such surface films cause less self-discharge that is initiated at the negative electrode. Negligible and constant self-discharge indicates that the ageing model based on OC storage mode tests data is as valid as the one based on charge sustaining (CS) mode tests, as assumed when defining the experimental conditions.

- Analysis of ageing mechanisms

Voltage profiles at different ageing stages and rate capability results indicated that LLI was induced over different storage conditions. LLI degradation mechanism was apparently the result of cell imbalance [2] due to different lithium consumption rate at negative and positive electrode. The graphite anode is the most

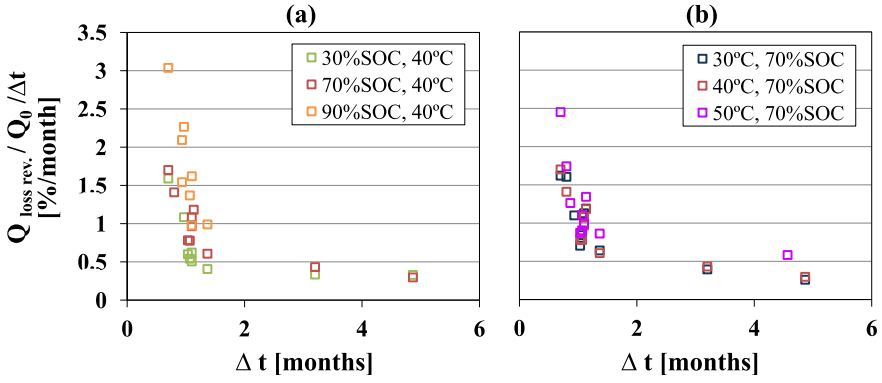

Fig. 8. The influence of SOC (a) and T (b) on cell self-discharge during OC storage. Reversible capacity loss rate (Q_{loss}) (normalised to initial nominal capacity, Q_0) depending on storing time interval duration (Δt).

critical electrode because it is not within the electrochemical stability window of the electrolyte [58], which provokes reduction of electrolyte and lithium oxidation at the anode surface. The resulting ionic conductive SEI passivation layer leads to LLI. At high temperature (50 °C, 70% SOC), not only was irreversible capacity loss measured, but also internal resistance increase (slight drop of voltage plateau in Fig. 4 and IR increase change in Fig. 5), which may also be the consequence of the growth of SEI layer containing complex electrochemically inactive products [3,54].

Analysis of incremental capacity (IC) and differential voltage (DV) curves derived from quasi-OCV measurements (described in section 2.1) enabled correlating graphite electrode material phase transformation reactions with degradation phenomena [77,78], as these curves are mainly representative of the graphite negative electrode in the case of LFP-based cell. The voltage curve of LFP presents a single plateau, which corresponds to $FePO_4$–$LiFePO_4$ phase transformation, that yields a featureless differentiation curve. Graphite, however, shows different plateaus on the charge–discharge potential profile that represent the coexistence of lithiated graphite at different Li_xC_6 transformation processes. Even though typically three-staging phenomena are reported for the graphite [6,71,78], for the studied LFP-based cell five of them were detected within graphite intercalation-deintercalation window coupled with LFP potential plateau, in agreement with observations of M. Dubarry *et al.* on LFP cells [74]. They are revealed as 5 valleys in DV curves in Fig. 9 (numbered as 1–5) for the different storage tests (the four peaks correspond to transitions between five transformation phases in equilibrium). M. Safari and C. Delacourt [22] reported four staging phenomena for the same cell configuration. Reduction of active lithium within the negative electrode at the beginning of cell discharge (graphite delithiation) was observed in all cases. The first valley in DV curves shrank gradually upon storage. This change of the stage 1 lithium-graphite compound most likely correspond to irreversible lithium loss (LLI) [71]. No other changes were particularly highlighted except for the cell stored at 50 °C and 70% SOC. Fig. 10 shows, more in detail, different ageing effects that were gradually detected upon storage on this cell. In this case, all peaks and valleys in IC and DV curves, respectively, somehow faded after prolonged storage even though the first valley in DV curves did not completely disappear. After 10–11 months of storage under 50 °C and 70% SOC, first peak in DV curves shifted to higher capacities reducing the distance between peaks. Likewise, not only the intensity of the peak at 3.32 V in IC curves (Fig. 10(a)) decreased so as for the one at 3.28 V. This effect

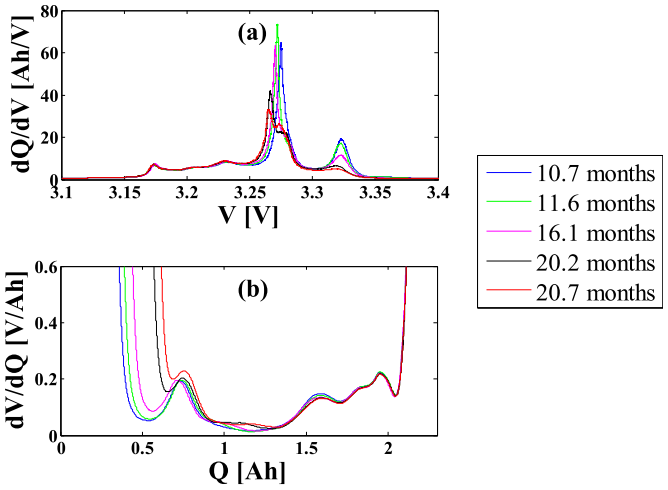

Fig. 10. IC (d*Q*/d*V*) (a) and DV (d*V*/d*Q*) (b) curves, obtained from C/5 discharge voltage profiles, for 50 °C and 70% SOC test after prolonged storage periods.

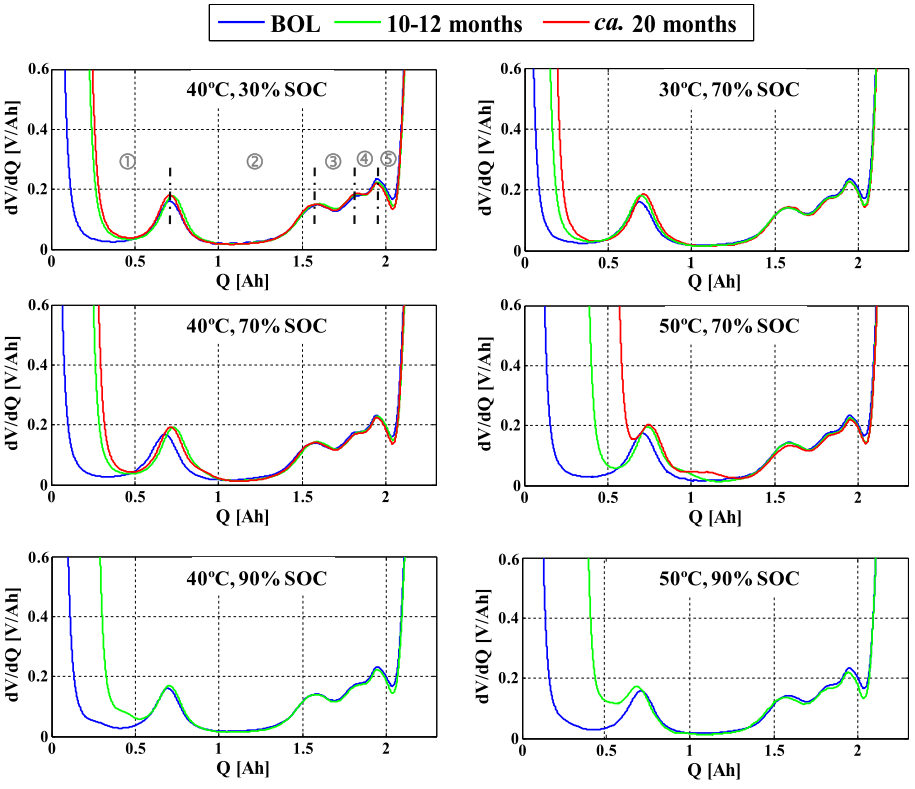

Fig. 9. Equivalent and representative DV curves, obtained from C/5 discharge voltage profiles, upon storage at different conditions.

represents loss of graphite active material (LAM), as the distance between any two peaks in DV curves is proportional to the amount of active carbon, *i.e.* capacity involved in the graphite electrode material phase transformation reactions [71,77,78]. Hence, loss in graphite available sites for reaction with lithium was induced, which means that graphite could not be lithiated to the same level as it was initially. The staging process would not however change, as none of the valleys in DV curves disappeared at all. Anyway, LLI was highly enhanced before LAM phenomenon was observed, so graphite LAM did not directly lead to capacity loss (there may be enough storage capacity for the amount of active lithium in the cell [71]). Hence, in this case graphite LAM could probably mean [22,74]: material dissolution, structural alteration, particle isolation, electrode delamination, etc. It is also reported that exfoliation and particle cracking due to solvent co-intercalation and electrolyte reduction inside graphite, sometimes accompanied with gas evolution, may occur, which would lead to rapid negative electrode deterioration [54].

From IC and DC curves it was not possible to find out the reasons for impedance change. EIS measurements were carried out with this purpose. In Fig. 11, a comparative study of 50 °C (70% SOC) storage condition with other at 30 °C (70% SOC) is shown, as it was deduced that cell resistance strongly depends on storage temperature. There are plotted EIS spectra measured at two different SOCs, aiming at confirming that the check-up SOC condition is not relevant for analysing cell impedance evolution. The approach for representative ageing effects identification is mainly focused on the observation of impedance real part changes at high and low frequency. The high frequency intercept with the real axis, related to ohmic resistance, was shifted to larger values, indicating degradation of electrolyte that leads to growth of SEI layer. The shift measured in the cell stored at 50 °C after just 3.7 months was similar to the one at 30 °C after *ca.* 21 months. It increased *ca.* 2 mOhm and *ca.* 0.5 mOhm at 50 °C and 30 °C storage, respectively, after *ca.* 21 months. Hence, the ohmic resistance change was highly influenced by cell ageing storage temperature. On the other hand, the semicircle resistance at medium frequency also changed significantly in the highly aged cell at 50 °C ambient temperature, in comparison with the one stored at 30 °C (*ca.* 21 months of storage). It means that apart from limiting the conductivity of electrolyte upon storage, as a result of its organic deposition on graphite electrode surface, the charge transfer was also limited as the passivating resistive layer got thicker and denser. These EIS observations correlate to DC IR sharp increase at prolonged storing times (Fig. 5, after the check-up at *ca.* 355 days of storage), as also concluded from quasi-OCV measurements.

Overall, in agreement with previous studies [22,44,79], calendar ageing close to room temperature (*e.g.* 30 °C in the present work) does not result in significant degradation of the electrode. Cell overall performance is limited by the available active lithium. After prolonged storage at high temperature, the results reveal that large LLI also led to LAM associated with graphite electrode and impedance change. LLI was responsible for the majority of ageing processes.

3.2. Calendar ageing prediction model

Lifetime of the investigated LFP-based cell, based on results discussed previously, would be restricted by the remaining available capacity (power fade would not be a limiting factor). Hence, the calendar ageing predictive model development is focused on capacity fade evolution. Five different storage conditions were used for modelling and an additional one, at the more severe conditions (50 °C and 90% SOC) for the static validation (Table 2). For the 50 °C and 70% SOC storage condition, the last 3 check-ups capacity results were not taken into account for impact factors effect quantification, since, as discussed above, there was a change in the dominant degradation mechanism, from LLI to a combination of LLI and LAM, after the check-up after 355 days of storage. A single degradation mode was modelled (LLI) as the appearance of the representative ageing effects changed upon ageing condition. Anyway, detecting the inflection points in experimental data, which indicate transition to sudden fade, is of high importance for defining the EOL. Otherwise, the lifetime would be over-predicted, as it can be observed in Fig. 12 (shadowed area).

Fig. 12 shows capacity loss experimental results (solid markers) at different accelerated ageing conditions, which were constant upon storage within each test, and the corresponding predictions (lines) resulting from the developed model. The static validation at 50 °C and 90% SOC is plotted in the same figure (dotted line). Lithium ions consumption rate, which is inversely proportional to the thickness of the SEI layer, followed the square root of time function [3]. The effect of storage temperature on chemical reactions that led to growth of SEI layer and the consequent impedance rise was explained by Arrhenius law. This law also takes into account the effect of cell voltage at high temperature and how it increases the rate of lithium loss [24]. The activation energy was 35.64 ± 19.35 kJ mol^{-1} (95% CI). Regarding voltage impact on parasitic chemical reactions leading to capacity loss, both linear [80] and exponential [24,81] evolutions were checked, providing the latter the best fitting in all cases. The proposed overall semi-

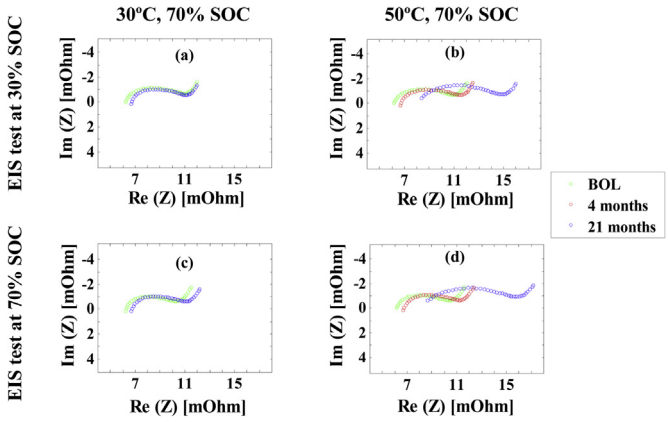

Fig. 11. EIS measurements of the cells stored at 50 °C and 70% SOC (a,c) and 30 °C and 70% SOC (b,d). EIS measurement at 25 °C and two different cell SOCs: 30% (a,b) and 70% (c,d).

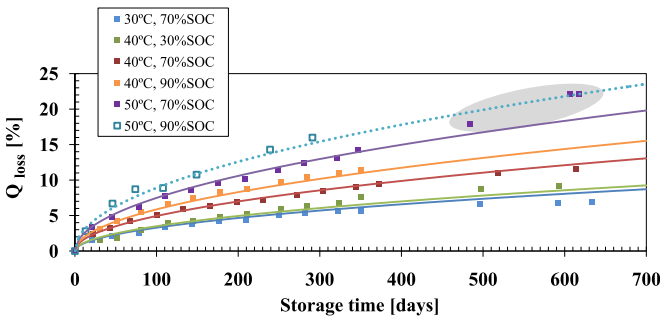

Fig. 12. Capacity loss (Q_{loss}) data at different storage static conditions (solid colour markers), fitted calendar degradation model (continuous lines). Open marker (50 °C, 90% SOC) corresponds to the test condition used for static validation and the dotted line is the model validation fit. (For interpretation of the references to colour in this figure legend, the reader is referred to the web version of this article.)

empiric mathematical model is as follows, where α_1, β_1, α_2 and β_2 are fitting parameters.

$$Q_{loss}\left[\%\right] = \alpha_1 \cdot \exp\left(\beta_1 \cdot T^{-1}\right) \cdot \alpha_2 \cdot \exp\left(\beta_2 \cdot SOC\right) \cdot t^{0.5} \quad (1)$$

The goodness of capacity loss fitting and prediction (validation) was evaluated for all experimental data point at each storage condition, but for data within shadowed area. The distribution of residuals is shown in Fig. 13 in a box plot, which includes the static validation prediction errors (*i.e.* data not used for modelling). The average values are indicated with open circles. Depicting graphically groups of numerical data through their quartiles enabled identifying outliers, which are marked with asterisks. They may be due to variability in the measurements or may indicate experimental error. The modelling accuracy was high for the 40 °C and 70% SOC condition. At this storing condition the variability was the least (boxes spacing), its distribution was negatively skewed and, additionally, the median residual (line inside the boxes) was the lowest. 40 °C and 90% SOC storing condition presented the largest median residual but it was similar to that of 40 °C and 30% SOC storing condition, which besides exhibited greater dispersion of residuals. .However, data at 70% SOC and different temperatures (30, 40 and 50 °C) showed very similar median residual: *ca.* 0.2%. Prediction at 30 °C exhibited the greatest variability among them with the distribution positively skewed, but its interquartile range was just about 0.4%. In conclusion, Fig. 13 indicates that temperature effect was very accurately quantified and the goodness of SOC impact factor modelling was slightly lower at the conditions that were not considered for temperature effect evaluation (30% and 90% SOC). In any case, even taking into account the variability outside the upper and lower quartiles (whiskers, *i.e.* lines extended from the boxes), the difference between measured data and estimation was not larger than 1%.

Static validation (50 °C, 90% SOC) showed that the largest verified prediction error was within the same range as for the model residuals, *ca.* 1% (Fig. 13). The median prediction error was larger than but similar to the median residual at 40 °C and 90% SOC storing condition. Taking into account that the validation consisted in very demanding storing conditions, it was concluded that the model demonstrated high degree of prediction accuracy and assumed that under other static storage conditions the predictions errors would be within the same range. Hence, the developed capacity loss model could be used for precise lifetime estimation within the analysed windows of SOC and T factors (Table 2) under such conditions.

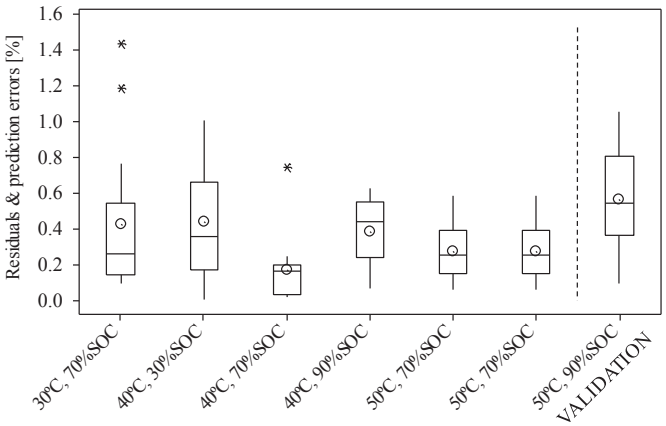

Fig. 13. Box plot of capacity loss prediction residuals and errors distribution for each storage condition.

- Model dynamic validation

As described earlier, the validity of the developed calendar-life predictive model was checked in other conditions different from the ones used for modelling (*i.e.* static validation at 50 °C and 90% SOC). Testing at constant operating conditions is not however enough for approaching cell behaviour in real applications, on which the operation and ambient temperature is dynamic. In order to enhance the applicability of the model, additional tests were carried out changing the impact factors within the profile on the same cell (Fig. 3). Fig. 14 shows experimental capacity loss data (diamond shaped symbols) of four cells (a-d) that were put to the test under different thermal and SOC profiles (in black lines) and the corresponding predictions using the developed calendar ageing model (in green lines). The method used for predicting the capacity loss at dynamic factors profiles took into account the accumulated ageing by former usage [82,83]. This way, the residual capacity was used as reference point for further predictions at different operating conditions and not simply the operating time.

From Fig. 13 it was deduced that temperature effect was more precisely quantified than SOC effect in the capacity loss predictive model. Fig. 14(d) shows that the average prediction error for dynamic SOC profiles upon storage on the same cell was 0.64%,

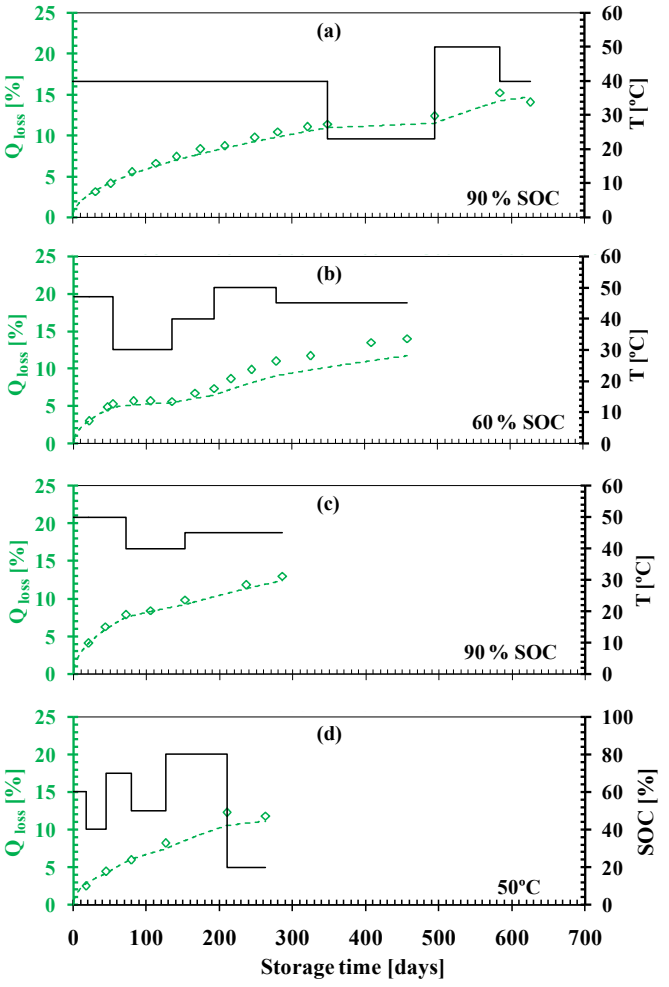

Fig. 14. Capacity loss (Q_{loss}) performance (diamond shaped symbols) under dynamic storage conditions for four tests (a–d, plotted in blue). The corresponding predictions are represented by green lines. (For interpretation of the references to colour in this figure legend, the reader is referred to the web version of this article.)

whereas it was 0.70% for dynamic temperature tests in Fig. 14(a–c). In any case, the overall root-mean-square error (RMSE) was just 0.93%, so the forecasting error at non-constant storage conditions was very low. Hence, it was comprehensively verified that:

(i) The prediction approach followed under random storage conditions, which considers the accumulated ageing over time at each condition, represents accurately the cell ageing.
(ii) It is possible to predict with high accuracy realistic cell performance loss under non-constant storage conditions using calendar ageing model based on constant conditions tests data. Hence, it is applicable for simulating eventual real effects of alternative conditions and courses of action, and analysing with low cost systems that cannot be engaged in a simple way.

The presented methodology is an effective way to obtain accurate calendar lifetime estimations under specific conditions of different real targeted applications. Focusing specially on dynamic validations enables reliable and cost-effective results. This way, the developed ageing predictive tool for the investigated LFP cell can be implemented with different simulation purposes. This work will be combined in subsequent papers with the cycling ageing analysis for joint lifetime prediction modelling.

The following section describes further estimations for an UPS application.

3.3. Real scenarios evaluation

The calendar life performance of a cell in worldwide UPS applications was evaluated. Three different scenarios located at Bangkok (Thailand), Jizan (Saudi Arabia) and Tenerife (Spain) were analysed. Average daily temperatures over a year [84–86] were considered as plotted in Fig. 15. It was supposed that the cell in the UPS would be at 90% SOC, ready to supply large power peaks. The SOC was considered constant upon storage for the predictions, as, after the very short runtime, the cell would be recharged immediately to the initial SOC when the power would turn back. It was also assumed that the activation energy of chemical reactions would not change above 15 °C up to 50 °C (such as it did barely between 30 and 50 °C). Fig. 16 shows the assessed capacity loss evolution over two years (the profiles in Fig. 15 were simulated twice). It was supposed that the initial main degradation mechanism (LLI) would not change, in agreement with previous observations. Experimental data at more demanding temperature conditions (40 °C and 90% SOC, and 50 °C and 90% SOC tests) only showed LLI over a year (Figs. 9 and 12). Furthermore, the model considering this ageing phenomena predicted precisely the capacity loss of a cell at non-constant temperature storage conditions during more than 600 days (Fig. 14(a),(c)).

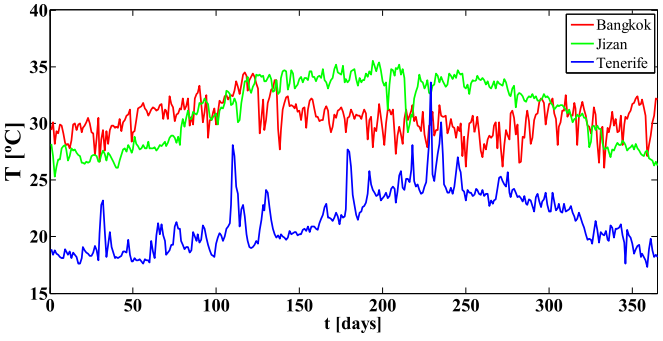

Fig. 15. Recorded average temperatures of Bangkok, Jizan and Tenerife for each day during one year.

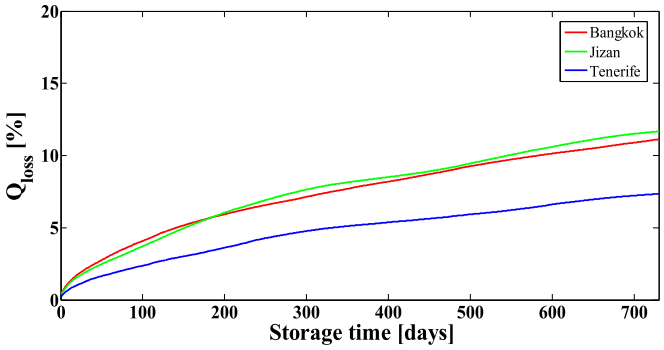

Fig. 16. Capacity loss (Q_{loss}) prediction for two years of operation at 90% SOC and temperature profiles in Fig. 15.

The capacity loss evolution of the battery stored in Jizan and Bangkok would be very similar as the thermal profiles are in these two cities. The largest average temperature difference between them over the year is 7.2 °C. Even though the temperature in Jizan is lower than in Bangkok during the first *ca.* 80 days of the year, the predicted cell capacity loss was larger in Bangkok even during the first 200 days. In agreement with the observed exponential dependence between temperature and evolved capacity loss (Fig. 12), initial higher storage temperature of just 2.5 °C in average would affect more the cell performance than thereafter average temperature difference of 3.5 °C during 200 days. After this period, however, for prolonged calendar time, the cell in the UPS of Jizan would be more degraded, even though the compared two thermal profiles change slightly (at the end of the year the temperature in Bangkok is slightly higher). In the case of the cell to be stored between 17 and 33 °C under the thermal profile measured in Tenerife, its capacity fade would be 4% lower after two years than for the ones stored between *ca.* 25–35 °C. The predicted capacity loss in a complete year was 5.2%, 7.9% and 8.3% at 21 °C, 30.5 °C and 31.9 °C median temperature, respectively. Hence, in this specific case, even though the differences are very low, the higher the median temperature, the larger the cell performance loss in the long-term.

4. Conclusions

The presented semi-empirical model successfully represents the storage behaviour of the cell both at static and dynamic operating conditions. The calculated model residuals and predictions under highly demanding static conditions are in all cases below 1%. The estimated RMSE for the dynamic validations under different T and SOC conditions over prolonged times is just 0.93%, corroborating the high model accuracy under realistic operating schemes. Dynamic validations enabled justifying the approach proposed for different real scenarios evaluation. They showed the relevance of following the initially defined methodology for the ageing model development, with special focus in the validation protocols, which in the end aims at a simple but robust and precise simulation tool with minimised experimental work.

The calendar ageing results indicated that the useful life of the investigated LFP-based Li-ion cell is mostly controlled by capacity fade rather than power fade. Hence, SOH monitoring and/or predicting should be based on the actual capacity, and the model is based on capacity loss evolution over time. Understanding of degradation was done by the combined analysis of voltage profiles, electric measurements of capacity and internal resistance ageing

metric, EIS measurements and IC and DV diagnostics techniques. The identified main ageing mechanism is LLI due to moderate SEI evolution. The SEI formation due to parasitic reactions in anode surface/electrolyte interface increases over time, also leading to cell impedance change. At high temperature and long storing time, additional ageing effects were induced and, as a consequence, the main degradation mechanism, initially LLI, changed to a combination of LLI and LAM. LAM ageing phenomenon accelerated dramatically the cell performance loss.

The developed semi-empirical model covers one main degradation mechanism (LLI) simulating square-root of time dependency, and both exponential SOC and temperature dependencies. The goodness of fit with the experimental results is very high and in most cases the model is able to predict calendar-ageing over a wide range of storage conditions. The simulation of the real UPS application proved that the events order within the dynamic thermal profiles determines the ageing upon storage. The developed model is able to adapt to the history of events.

Acknowledgement

This investigation work was financially supported by ETORTEK (Energigune'12 - I+D+i en almacenamiento de energía electroquímica y térmica, y en energía marina, IE12-335) and EMAITEK Strategic Programs of the Basque Government.

References

[1] A. Eddahech, O. Briat, E. Woirgard, J.M. Vinassa, Microelectron. Reliab. 52 (2012) 2438–2442.
[2] S. Grolleau, A. Delaille, H. Gualous, P. Gyan, R. Revel, J. Bernard, E. Redondo-Iglesias, J. Peter, J. Power Sources 255 (2014) 450–458.
[3] M. Broussely, S. Herreyre, P. Biensan, P. Kasztejna, K. Nechev, R.J. Staniewicz, J. Power Sources 97–98 (2001) 13–21.
[4] J. Belt, V. Utgikar, I. Bloom, J. Power Sources 196 (2011) 10213–10221.
[5] M. Kassem, J. Bernard, R. Revel, S. Pélissier, F. Duclaud, C. Delacourt, J. Power Sources 208 (2012) 296–305.
[6] D.P. Abraham, J. Liu, C.H. Chen, Y.E. Hyung, M. Stoll, N. Elsen, S. MacLaren, R. Twesten, R. Haasch, E. Sammann, I. Petrov, K. Amine, G. Henriksen, J. Power Sources 119–121 (2003) 511–516.
[7] R.P. Ramasamy, R.E. White, B.N. Popov, J. Power Sources 141 (2005) 298–306.
[8] R.B. Wright, C.G. Motloch, J.R. Belt, J.P. Christophersen, C.D. Ho, R.A. Richardson, I. Bloom, S.A. Jones, V.S. Battaglia, G.L. Henriksen, T. Unkelhaeuser, D. Ingersoll, H.L. Case, S.A. Rogers, R.A. Sutula, J. Power Sources 110 (2002) 445–470.
[9] K. Amine, J. Liu, I. Belharouak, Electrochem. Commun. 7 (2005) 669–673.
[10] K. Amine, C.H. Chen, J. Liu, M. Hammond, A. Jansen, D. Dees, I. Bloom, D. Vissers, G. Henriksen, J. Power Sources 97–98 (2001) 684–687.
[11] I. Bloom, B.W. Cole, J.J. Sohn, S.A. Jones, E.G. Polzin, V.S. Battaglia, G.L. Henriksen, C. Motloch, R. Richardson, T. Unkelhaeuser, D. Ingersoll, H.L. Case, J. Power Sources 101 (2001) 238–247.
[12] D. Aurbach, B. Markovsky, A. Rodkin, E. Levi, Y.S. Cohen, H.J. Kim, M. Schmidt, Electrochim. Acta 47 (2002) 4291–4306.
[13] R.G. Jungst, G. Nagasubramanian, H.L. Case, B.Y. Liaw, A. Urbina, T.L. Paez, D.H. Doughty, J. Power Sources 119–121 (2003) 870–873.
[14] K. Asakura, M. Shimomura, T. Shodai, J. Power Sources 119–121 (2003) 902–905.
[15] B. Markovsky, Y. Talyossef, G. Salitra, D. Aurbach, H.J. Kim, S. Choi, Electrochem. Commun. 6 (2004) 821–826.
[16] R.P. Ramasamy, J.W. Lee, B.N. Popov, J. Power Sources 166 (2007) 266–272.
[17] S. Käbitz, J.B. Gerschler, M. Ecker, Y. Yurdagel, B. Emmermacher, D. André, T. Mitsch, D.U. Sauer, J. Power Sources 239 (0) (2013) 572–583.
[18] M. Ecker, J.B. Gerschler, J. Vogel, S. Käbitz, F. Hust, P. Dechent, D.U. Sauer, J. Power Sources 215 (2012) 248–257.
[19] Q. Zhang, R.E. White, J. Power Sources 173 (2007) 990–997.
[20] Q. Zhang, R.E. White, J. Power Sources 179 (2008) 785–792.
[21] M. Ecker, N. Nieto, S. Käbitz, J. Schmalstieg, H. Blanke, A. Warnecke, D.U. Sauer, J. Power Sources 248 (2014) 839–851.
[22] M. Safari, C. Delacourt, J. Electrochem. Soc. 158 (2011) A1123–A1135.
[23] C. Delacourt, M. Safari, J. Electrochem. Soc. 159 (2012) A1283–A1291.
[24] R. Arunachala, in: RWTH Aachen university, 2011.
[25] I. Bloom, S.A. Jones, V.S. Battaglia, G.L. Henriksen, J.P. Christophersen, R.B. Wright, C.D. Ho, J.R. Belt, C.G. Motloch, J. Power Sources 124 (2003) 538–550.
[26] B.Y. Liaw, E.P. Roth, R.G. Jungst, G. Nagasubramanian, H.L. Case, D.H. Doughty, J. Power Sources 119–121 (2003) 874–886.
[27] E.V. Thomas, H.L. Case, D.H. Doughty, R.G. Jungst, G. Nagasubramanian, E.P. Roth, J. Power Sources 124 (2003) 254–260.
[28] D.P. Abraham, in: Argonne National Laboratory, U.S. Department of Energy, 2005.
[29] Y. Mita, S. Seki, N. Terada, N. Kihira, K. Takei, H. Miyashiro, Electrochem. Commun. 78 (2010) 384–386.
[30] G. Sarre, P. Blanchard, M. Broussely, J. Power Sources 127 (2004) 65–71.
[31] T. Yoshida, M. Takahashi, S. Morikawa, C. Ihara, H. Katsukawa, T. Shiratsuchi, J.-i. Yamaki, J. Electrochem. Soc. 153 (2006) A576–A582.
[32] I. Bloom, L.K. Walker, J.K. Basco, D.P. Abraham, J.P. Christophersen, C.D. Ho, J. Power Sources 195 (2010) 877–882.
[33] I. Bloom, B.G. Potter, C.S. Johnson, K.L. Gering, J.P. Christophersen, J. Power Sources 155 (2006) 415–419.
[34] J.P. Christophersen, C.D. Hoa, C.G. Motloch, D. Howell, H.L. Hess, J. Electrochem. Soc. 153 (2006) A1406–A1416.
[35] B. Lunz, Z. Yan, J.B. Gerschler, D.U. Sauer, Energy Policy 46 (2012) 511–519.
[36] M.C. Smart, B.V. Ratnakumar, L.D. Whitcanack, F.J. Puglia, S. Santee, R. Gitzendanner, Int. J. Energy Res. 34 (2010) 116–132.
[37] B.Y. Liaw, R.G. Jungst, G. Nagasubramanian, H.L. Case, D.H. Doughty, J. Power Sources 140 (2005) 157–161.
[38] M. Klett, R. Eriksson, J. Groot, P. Svens, K. Ciosek Högström, R.W. Lindström, H. Berg, T. Gustafson, G. Lindbergh, K. Edström, J. Power Sources 257 (2014) 126–137.
[39] E.V. Thomas, E.P. Roth, D.H. Doughty, R.G. Jungst, in: Sandia National Laboratories, 2003.
[40] E.V. Thomas, I. Bloom, J.P. Christophersen, V.S. Battaglia, J. Power Sources 184 (2008) 312–317.
[41] D. Aurbach, B. Markovsky, Y. Talyossef, G. Salitra, H.-J. Kim, S. Choi, J. Power Sources 162 (2006) 780–789.
[42] J. Schmalstieg, S. Käbitz, M. Ecker, D.U. Sauer, J. Power Sources 257 (2014) 325–334.
[43] M. Dubarry, C. Truchot, B.Y. Liaw, K. Gering, S. Sazhin, D. Jamison, C. Michelbacher, J. Power Sources 196 (2011) 10336–10343.
[44] T.G. Zavalis, M. Klett, M.H. Kjell, M. Behm, R.W. Lindström, G. Lindbergh, Electrochim. Acta 110 (2013) 335–348.
[45] B. Stiaszny, J.C. Ziegler, E.E. Krauß, J.P. Schmidt, E. Ivers-Tiffée, J. Power Sources 251 (2014) 439–450.
[46] M. Kassem, C. Delacourt, J. Power Sources 235 (2013) 159–171.
[47] M. Safari, C. Delacourt, J. Electrochem. Soc. 158 (2011) A1436–A1447.
[48] I. Bloom, J. Christophersen, K. Gering, J. Power Sources 139 (2005) 304–313.
[49] X.V. Zhang, P.N. Ross, R. Kostecki, F. Kong, S. Sloop, J.B. Kerr, K. Striebel, E.J. Cairns, F. McLarnon, J. Electrochem. Soc. 148 (2001) A463–A470.
[50] S. Bourlot, P. Blanchard, S. Robert, J. Power Sources 196 (2011) 6841–6846.
[51] S. Watanabe, M. Kinoshita, K. Nakura, J. Power Sources 247 (2014) 412–422.
[52] I. Bloom, J.P. Christophersen, D.P. Abraham, K.L. Gering, J. Power Sources 157 (2006) 537–542.
[53] M. Broussely, P. Biensan, F. Bonhomme, P. Blanchard, S. Herreyre, K. Nechev, R.J. Staniewicz, J. Power Sources 146 (2005) 90–96.
[54] J. Vetter, P. Novák, M.R. Wagner, C. Veit, K.C. Möller, J.O. Besenhard, M. Winter, M. Wohlfahrt-Mehrens, C. Vogler, A. Hammouche, J. Power Sources 147 (2005) 269–281.
[55] P. Arora, M. Doyle, R.E. White, J. Electrochem. Soc. 146 (1999) 3543–3553.
[56] D. Stroe, M. Swierczynski, A.-I. Stan, R. Teodorescu, 2013 IEEE, in: Energy Conversion Congress and Exposition (ECCE), IEEE, Denver, CO, 2013, pp. 690–698.
[57] H. Joachin, T.D. Kaun, K. Zaghib, J. Prakash, J. Electrochem. Soc. 156 (2009) A401–A406.
[58] B. Scrosati, J. Garche, J. Power Sources 195 (2010) 2419–2430.
[59] A.K. Padhi, K.S. Nanjundaswamy, J.B. Goodenough, J. Electrochem. Soc. 144 (1997) 1188–1194.
[60] A. Yamada, S.C. Chung, K. Hinokuma, J. Electrochem. Soc. 148 (2001) A224–A229.
[61] N. Ravet, Y. Chouinard, J.F. Magnan, S. Besner, M. Gauthier, M. Armand, J. Power Sources 97–98 (2001) 503–507.
[62] H. Huang, S.C. Yin, L.F. Nazar, Electrochem. Solid State Lett. 4 (2001) A170–A172.
[63] Z. Chen, J.R. Dahn, J. Electrochem. Soc. 149 (2002) A1184–A1189.
[64] S.Y. Chung, J.T. Bloking, Y.M. Chiang, Nat. Mater. 1 (2002) 123–128.
[65] S. Franger, F.L. Cras, C. Bourbon, H. Rouault, J. Electrochem. Soc. 151 (2004) A1024–A1027.
[66] A. Ritchie, W. Howard, J. Power Sources 162 (2006) 809–812.
[67] E. Sarasketa-Zabala, I. Laresgoiti, I. Alava, M. Rivas, I. Villarreal, F. Blanco, in: EVS27, Barcelona, Spain, 2013.
[68] E.V. Thomas, I. Bloom, J.P. Christophersen, V.S. Battaglia, J. Power Sources 206 (2012) 378–382.
[69] T. Utsunomiya, O. Hatozaki, N. Yoshimoto, M. Egashira, M. Morita, J. Power Sources 196 (2011) 8675–8682.
[70] M. Dubarry, B.Y. Liaw, M.S. Chen, S.S. Chyan, K.C. Han, W.T. Sie, S.H. Wu, J. Power Sources 196 (2011) 3420–3425.
[71] P. Liu, J. Wang, J. Hicks-Garner, E. Sherman, S. Soukiazian, M. Verbrugge, H. Tataria, J. Musser, P. Finamore, J. Electrochem. Soc. 157 (2010) A499–A507.
[72] J. Groot, in: Division of Electric Power Engineering, Department of Energy and Environment, Chalmers University of Technology Göteborg, Sweden, 2012.

[73] G. Gachot, S. Grugeon, G.G. Eshetu, D. Mathiron, P. Ribière, M. Armand, S. Laruelle, Electrochim. Acta 83 (2012) 402–409.
[74] M. Dubarry, B.Y. Liaw, J. Power Sources 194 (2009) 541–549.
[75] S.S. Zhang, K. Xu, T.R. Jow, J. Power Sources 115 (2003) 137–140.
[76] R. Yazami, Y.F. Reynier, Electrochim. Acta 47 (2002) 1217–1223.
[77] M. Dubarry, C. Truchot, B.Y. Liaw, J. Power Sources 219 (2012) 204–216.
[78] X. Han, M. Ouyang, L. Lu, J. Li, Y. Zheng, Z. Li, J. Power Sources 251 (2014) 38–54.
[79] M. Hellqvist Kjell, S. Malmgren, K. Ciosek, M. Behm, K. Edström, G. Lindbergh, J. Power Sources 243 (2013) 290–298.
[80] F. Herb, A. Frank, C. Nitsche, A. Jossen, Optimierung der regelung zwischen brennstoffzelle und batterie in bezug auf komponentenalterung, vol. 57, 2009, pp. 40–47.
[81] A. Barré, B. Deguilhem, S. Grolleau, M. Gérard, F. Suard, D. Riu, J. Power Sources 241 (2013) 680–689.
[82] M. Lepiorz, W. Weydanz, D. Most, A. Jossen, in: 5th Advanced Battery Power Aachen, Germany, 2013.
[83] H. Wenzl, A. Haubrock, H.P. Beck, Z. fur Phys. Chem. 227 (2013) 57–71.
[84] http://www.tutiempo.net/clima/BANGKOK/2013/484550.htm (accessed 24.04.14).
[85] http://www.tutiempo.net/clima/Gizan/2013/411400.htm (accessed 24.04.14).
[86] http://www.tutiempo.net/clima/Tenerife_Sur/2013/600250.htm (accessed 24.04.14).

Glossary

BOL: beginning of life
CC: constant current
CV: constant voltage
quasi-OCV: close-to-equilibrium open circuit voltage
Q: actual capacity. Cell0027s available capacity
Q_0: initial capacity
Q_{loss}: capacity loss CI confidence interval
C-rate: current rate, referred to the nominal capacity of the cell
DC IR: direct current internal resistance
DOD: depth of discharge
DV: differential voltage
EIS: electrochemical impedance spectroscopy
E_{loss}: energy loss
EOL: end of life
EOT: end of test
EPIT: electrical parameters identification tests
ESS: energy storage systems
EV: electric vehicle
HEV: hybrid electric vehicle
HPPT: hybrid pulse power test
IC: incremental capacity
IR: actual internal resistance
IR_0: initial internal resistance
$IR_{increase}$: internal resistance increase
LCO: lithium cobalt oxide, $LiCoO_2$ (cathode chemistry)
LFP: lithium iron phosphate, $LiFeOP_4$ (cathode chemistry)
LIB: Li-ion battery
Li-ion: lithium ion
LAM: loss of active material
LLI: loss of lithium inventory
LMO: lithium manganese oxide spinel, $LiMn_2O_4$ (cathode chemistry)
LNCO: lithium nickel cobalt oxide, $LiNiCoO_2$ (cathode chemistry)
N: number of cycles
NCA: lithium nickel cobalt aluminium oxide, $LiNiCoAlO_2$ (cathode chemistry)
NMC: lithium nickel manganese cobalt oxide, $Li(NiMnCo)O_2$ (cathode chemistry)
NMO: lithium manganese nickel oxide, $Li(NiMn)_2O_4$ (cathode chemistry)
OC: open circuit
SEI: solid electrolyte interface
SOC: state of charge
SOH: state of health
T: temperature
UPS: uninterruptible power supply